

DOI 10.24425/ae.2025.153020

Study on the influence of three-phase voltage unbalance on electromagnetic performance and vibration of high-voltage line-start permanent magnet synchronous motor

CUNXIANG YANG¹, JICHAO JIA¹✉, JIANING LIANG¹, ZHENJIANG WANG¹, HONGBO QIU²

¹College of Building Environment Engineering, Zhengzhou University of Light Industry
Zhengzhou city, Henan, China

²College of Electric and Information Engineering, Zhengzhou University of Light Industry
Zhengzhou city, Henan, China

e-mail: {yangzha/qiuhongbo}@zzuli.edu.cn, {✉ 2648228203/1160214722/110975005}0@qq.com

(Received: 28.06.2024, revised: 10.02.2025)

Abstract: Since the operation of the high-voltage line-start permanent magnet synchronous motor (HVLSPMSM) does not need the control circuit and is directly powered by the grid, its operating stability is easily affected by the three-phase voltage unbalance. Thus, a 10 kV, 630 kW motor is taken as an example to study the impact of voltage unbalance on its electromagnetic performance and vibration. First, the effect of voltage unbalance on the torque performance of the motor is investigated using the finite element method (FEM), and the variation rules of torque ripple and torque harmonic frequency with voltage unbalance degree are obtained. Then, the analytical expressions of radial electromagnetic force (REF) under normal and unbalanced voltage conditions are derived, and the rules of electromagnetic force variation of different orders and frequencies under rated load and unbalanced voltage conditions are determined, and the analytical results are verified by finite element results. Finally, the motor vibration response characteristics caused by three-phase voltage unbalance are obtained by using modal analysis and vibration harmonic response analysis. The results indicate that the vibration performance of the motor is significantly affected by the three-phase voltage unbalance. When the voltage unbalance degree is 6%, a vibration acceleration amplitude of 800 Hz and 900 Hz increases by 18.03% and 78.57%, respectively.

Key words: modal, radial electromagnetic force, torque harmonics, torque ripple, vibration harmonic response



© 2025. The Author(s). This is an open-access article distributed under the terms of the Creative Commons Attribution-NonCommercial-NoDerivatives License (CC BY-NC-ND 4.0, <https://creativecommons.org/licenses/by-nc-nd/4.0/>), which permits use, distribution, and reproduction in any medium, provided that the Article is properly cited, the use is non-commercial, and no modifications or adaptations are made.

1. Introduction

The high-voltage line-start permanent magnet synchronous motor (HVLSPMSM) has been widely applied in various industries, mainly due to its combination of the simplicity of operation and easy maintenance of induction motors, as well as the high efficiency of the PMSM [1,2]. The stator structure of the LSPMSM is the same as that of the conventional induction machine, and the rotor contains a permanent magnet (PM) and squirrel-cage guide bar structure, and the special rotor structure feature enables the motor to realize line-start by the squirrel-cage guide bar [3,4]. Its normal operation does not require additional control circuits and it is directly powered by the grid. The operating stability of the HVLSPMSM is easily affected by three-phase voltage unbalance. Thus, studying the impact of three-phase voltage imbalance on the performance of the LSPMSM is of great significance.

For three-phase voltage unbalance of the motor, domestic and foreign experts and scholars have done a great number of researches. In Reference [5], the line voltage unbalance coefficient, phase voltage unbalance coefficient and voltage unbalance coefficient are compared and analyzed for evaluating voltage asymmetry. In Reference [6], an instantaneous simulation model is established based on MATLAB, and the variation rules of motor starting time, current unbalance factor and torque ripple under different voltage unbalance rates are obtained. In Reference [7], the impact of voltage reduction on the starting operating capacity of the motor is studied. In Reference [8], a dynamic model of the LSPMSM is established through Simulink, and the influence of short-term interruption of three-phase voltage and transient voltage drop on the operating capacity before and after starting are analyzed. In Reference [9], the dynamic model and the DTC model of the motor are established through Simulink and the impact of voltage drop on the starting performance of the motor under different control modes is studied. In Reference [10], the transient and steady-state performance of the induction motor is studied by a complex unbalance factor. In References [11] and [12], the steady-state operating capacity of the motor is analyzed by using the equivalent circuit.

Existing researches on three-phase voltage unbalance are mainly aimed at induction motor, the research on HVLSPMSM is less. The power factor, starting operating capacity, operating efficiency and temperature rise of the motor were studied more, but the operation stability and vibration of the motor studied less. Therefore, a 10 kV, 630 kW HVLSPMSM is chosen as the research object in this study, which analyzes the influence of voltage unbalance on the motor torque, the REF and vibration harmonic response.

2. The definition of voltage unbalance and the establishment and experimental verification of finite element model

2.1. Definition of voltage unbalance

The measurement of voltage unbalance degree generally has three definitions given by the IEEE, NEMA and IEC [13]. These definitions are usually divided into the following eight cases: single-phase undervoltage, two-phase undervoltage, three-phase undervoltage; single-phase, two-phase, three-phase overvoltage; and the phase angular displacement of single-phase and two-phase. In this study, the research focuses on the voltage unbalance resulting from single-phase

overvoltage. Since the phase-voltage is easy to measure in the experiment, the degree of voltage unbalance (VUD) can be defined by the following formula [13]:

$$\begin{cases} \text{VUD}(\%) = \frac{\text{Max} [|U_A - U_{\text{avg}}| \cdot |U_B - U_{\text{avg}}| \cdot |U_C - U_{\text{avg}}|]}{U_{\text{avg}}} \times 100\% \\ U_{\text{avg}} = \frac{U_A + U_B + U_C}{3} \end{cases}, \quad (1)$$

where VUD(%) is the three-phase voltage unbalance degree, and U_A , U_B , U_C are the voltages of phase A, phase B and phase C, respectively; and U_{avg} is the average value of the three-phase voltage.

2.2. Model and parameters

A 10 kV, 630 kW HVLSPMSM is chosen as the research object in this study. The main parameters of the HVLSPMSM are displayed in Table 1. A two-dimensional finite element model is established according to the motor parameters of Table 1, as shown in Fig. 1.

Table 1. Main parameters of the motor

Parameters	Value
Rated power	630 kW
Rated speed	750 r/min
Rated voltage	10 kV
Number of poles	8
Axial length of the core	710 mm
Outer diameter of stator (R_{st})	880 mm
Inner diameter of stator (R_{ro})	600 mm
Inner diameter of rotor (R_{sh})	360 mm
Number of stator slots	72
Number of rotor slots	56
Air-gap size	2.5 mm

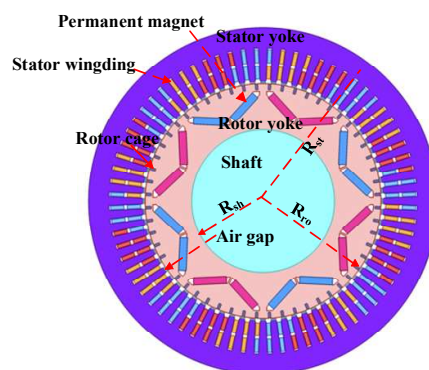


Fig. 1. Two-dimensional FEM the HVLSPMSM

2.3. Correctness verification of the model

To validate the correctness of the two-dimensional finite element model of HVLSPMSM, a test platform of the prototype was built, as shown in Fig. 2. These test results include power factor, no-load back electromotive force, rated current, no-load current and copper loss. These results were compared with those calculated by the FEM, as shown in Table 2.



Fig. 2. Motor experiment platform

Table 2. Comparison of finite element results and experimental results

Parameters	Experimental data	Finite element data	Variation rate (%)
Rated load current	38.5 A	38.6 A	0.25
Power factor	0.981	0.985	0.40
EMF	5.024 kV	5.36 kV	6.69
No-load current	6.6 A	6.58 A	0.30
Copper loss	5.87 kW	5.75 kW	2.04

According to Table 2, the errors of rated load current, power factor, no-load back electromotive force, no-load current and copper loss of the HVLSPMSM are all within 7%. The test result of the machine is basically consistent with the finite element result, which validates the correctness of the finite element model of 10 kV, 630 kW HVLSPMSM.

3. The effect on the torque performance

When the motor is operating the rated load, torque is produced by the interaction of the fundamental magnetic field, and it is a constant torque. However, due to the harmonic component of the magnetomotive force, the interaction between the stator harmonic magnetomotive force

and the rotor harmonic magnetomotive force can generate additional ripple torque, which is superimposed on the constant torque and causes the motor torque ripple. Under the three-phase voltage unbalance conditions, the stator winding current contains not only the positive sequence component but also some of the negative sequence component. At this time, the stator winding magnetomotive force can be divided into positive sequence and negative sequence magnetomotive force. The torque ripple will also alter due to the change in the variation of the synthesized magnetomotive force of the stator winding.

To more accurately analyze the torque ripple, definition Formula (2) calculates the torque ripple. The FEM was used to compare the torque ripple under different VUDs, and the results are shown in Fig. 3.

$$T_{\text{rip}} = \left| \frac{T_{\text{max}} - T_{\text{min}}}{2T_{\text{avg}}} \right| \times 100\%, \quad (2)$$

where T_{rip} is the torque ripple, T_{max} is the max torque in a period, T_{min} is the min torque in a period, and T_{avg} is the average torque in a period.

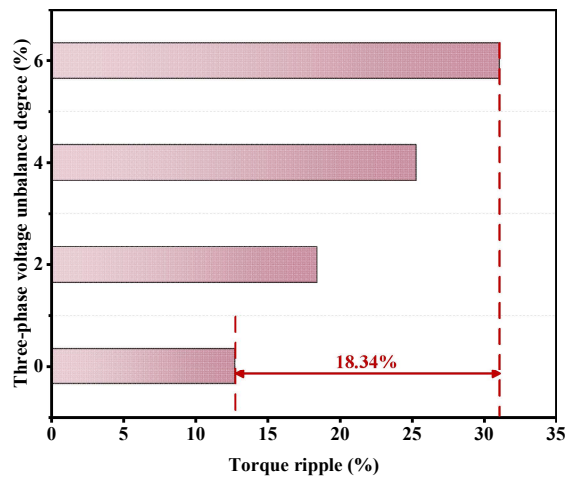


Fig. 3. Torque ripple of the motor

According to Fig. 3, under rated load condition, the torque ripple is 12.72%. Under the voltage unbalance condition, the torque ripple increases significantly, and the torque ripple increases with the increase in the VUD. The VUD is 6%, the torque ripple is 31.06%, which increases by 18.34% compared with the rated load condition.

The motor's three-phase voltage unbalance will not only generate a large torque ripple but also affect the harmonic components in the torque. Thus, it is necessary to study the impact of voltage unbalance on the harmonic components of the torque.

The torque is the synthesis of the torque produced by the interaction between the stator and the rotor magnetomotive force (MMF). The stator MMF of the motor can be expressed as [14]:

$$\begin{cases} F_A(\theta, t) = \sum_{v=1,3,5}^{\infty} F_v \cos(v\theta) \cos(\omega_1 t) \\ F_B(\theta, t) = \sum_{v=1,3,5}^{\infty} F_v \cos[v(\theta - 120^\circ) \cos(\omega_1 t - 120^\circ)] , \\ F_C(\theta, t) = \sum_{v=1,3,5}^{\infty} F_v \cos[v(\theta + 120^\circ) \cos(\omega_1 t + 120^\circ)] \end{cases} \quad (3)$$

where v is the order of the harmonic component; F_v is the v -th harmonic component amplitude of the stator MMF; θ is the spatial angle.

The harmonic MMF of the rotor is:

$$F_m(\theta t) = \sum_{v=1,3,5}^{\infty} F_{mv} \cos(v\theta - v\omega_1 t - \varphi_v), \quad (4)$$

where φ_v is the phase angle difference of the v -harmonic MMF of the stator and rotor.

The three-phase stator MMF of the motor interacts with the rotor MMF respectively to generate torque. The torque expression is shown in the following equation [15]:

$$\begin{aligned} T_{Av} &= \frac{1}{2} v K F_v F_{mv} \{ \sin[(v \mp 1)\omega t + \varphi_v] + \sin[(v \pm 1)\omega t + \varphi_v] \} \\ T_{Bv} &= \frac{1}{2} v K F_v F_{mv} \{ \sin[(v \mp 1)\omega t + \varphi_v] + \sin[(v \pm 1)\omega t + \varphi_v \mp 240^\circ] \}, \\ T_{Cv} &= \frac{1}{2} v K F_v F_{mv} \{ \sin[(v \mp 1)\omega t + \varphi_v] + \sin[(v \pm 1)\omega t + \varphi_v \pm 240^\circ] \} \end{aligned} \quad (5)$$

$$K = (\mu_0 \pi D_g l_a) / (2g). \quad (6)$$

Combined with the above formulas, the synthetic torque expression of the three-phase stator and rotor MMF can be obtained [15]:

$$T_v = T_{Av} + T_{Bv} + T_{Cv} = \frac{3}{2} v K F_v F_{mv} \sin[(v \mp 1)\omega t + \varphi_v], \quad (7)$$

where $v = 6k \pm 1$, $k = 0, 1, 2, \dots$; g is the length of the air-gap; D_g is the average air-gap diameter; l_a is the axial length of the stator core.

From the above theoretical analysis, when the motor is operating under rated load, only $6k$ ($k = 1, 2, 3, \dots$) torque components are produced. However, when the voltage unbalance occurs, there is a part of the negative sequence component in the current, and the fundamental magnetic field produced by the negative sequence component interacts with the fundamental magnetic field of the rotor, resulting in a ripple frequency of $2f_1$ in the torque. In the same case, when the harmonic magnetic field generated by the negative sequence component interacts with the harmonic magnetic field of the rotor, the ripple torque will also be generated, and the ripple frequency is an even multiple of the fundamental component of the torque. In summary, it can be concluded that the negative sequence current makes a torque harmonic component of $2n$ ($n = 1, 2, 3, \dots$) times appear.

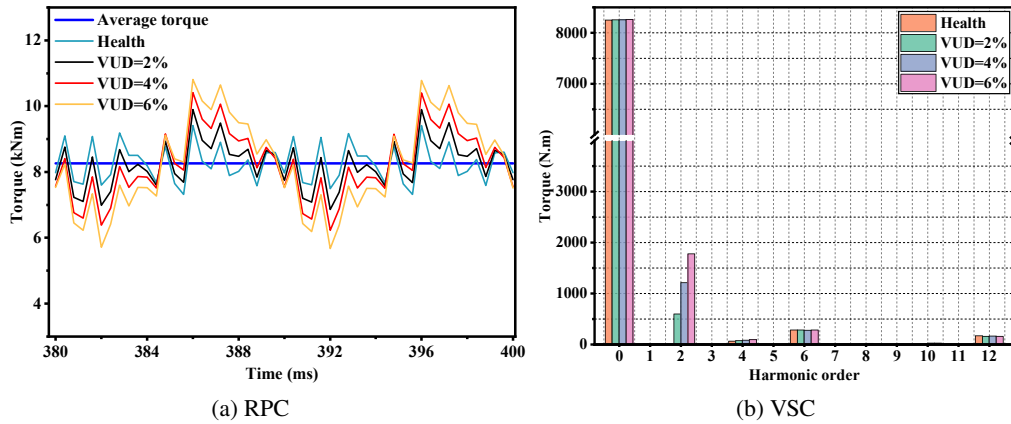


Fig. 4. Torque change curves and Fourier decomposition results under different VUDs

The torque change curves on different VUDs were obtained by the FEM, and the Fourier decomposition is performed on them. The results are shown in Fig. 4.

From Fig. 4, when the motor is operating under rated load condition, the torque harmonic component of the motor is mainly 6, 12 times, which is $6kf$. When the three-phase voltage unbalance occurs, the torque harmonic component contains 2, 4, 6, 12 times, which is $2nf$. The above theoretical analysis is well verified. The amplitude of the 2-th torque harmonic component is larger, and its amplitude increases with the increase in the VUD.

4. The effect on radial electromagnetic force

The REF generated by the interaction of stator and rotor magnetic fields is the main vibration source of the motor. According to magnetomotive force and the permeability method, the magnetic field is mainly determined by the magnetomotive force and permeability. Thus, to deeply study the electromagnetic vibration of the motor, it is essential to focus on the MMF and the air gap permeability, and analyze the multi-harmonic magnetic field and the REF produced by the interaction of these magnetic fields.

The MMF of the rotor PM can be expressed as:

$$f_{\mu}(\theta t) = F_{\mu} \cos(\mu\theta - \mu\omega_r t - \varphi_2), \quad (8)$$

where μ is the harmonic order of the PM magnetomotive force; $\mu = (2k + 1)p$ and F_{μ} is the amplitude of the magnetomotive force of the PM.

The v -th harmonic synthesized magnetomotive force of symmetric three-phase winding can be expressed as:

$$\begin{aligned} f_v &= f_{Av} + f_{Bv} + f_{Cv} \\ &= F_{\phi v} \cos v\theta_s \cos \omega t + F_{\phi v} \cos v(\theta_s - 120^\circ) \cos(\omega t - 120^\circ) \\ &\quad + F_{\phi v} \cos v(\theta_s - 120^\circ) \cos(\omega t - 120^\circ). \end{aligned} \quad (9)$$

The synthesized MMF of the stator can be expressed as:

$$f_v(\theta t) = \sum F_v \cos(vp\theta + \omega_1 t + \varphi) + \sum F_v \cos(vp\theta - \omega_1 t + \varphi). \quad (10)$$

Since the HVLSPMSM is a combination of the asynchronous motor and PMSM, which is convenient for subsequent electromagnetic force calculation, the synthesized MMF of the stator can be expressed as:

$$f_v(\theta t) = F_m \cos(v\theta - \omega_1 t - \varphi_1), \quad (11)$$

where F_m is the amplitude of the stator MMF, v is the order of the MMF of the stator winding, $v = (6k + 1)p$, $k = 0, 1, 2, \dots$, ω_1 is the synchronous angular frequency, $\omega_1 = p\omega_r$.

Compared with the single-slot PMSM, the LSPMSM air gap permeability not only contains the constant component of the air-gap permeability and the slotted stator permeability but adds the rotor tooth permeability component. Ignoring the permeability caused by the stator and rotor slotted, the air-gap permeability can be expressed as [16]:

$$\lambda_{k_1 k_2} = \Lambda_0 + \sum_{k_1} \Lambda_{k_1} \cos k_1 Z_1 \theta + \sum_{k_2} \Lambda_{k_2} \cos k_2 Z_2 (\theta - \omega_r t), \quad (12)$$

where ω_r is the rotor mechanical angular frequency; Λ_{k_1} is the amplitude of the k_1 -th stator permeability harmonic; Λ_{k_2} is the amplitude of the k_2 -th rotor permeability harmonic. Z_1 is the number of stator slots. Z_2 is the number of rotor slots.

When the motor is operating under rated load condition, the air-gap MMF can be obtained:

$$f_s = \sum_v F_v \cos(v\theta - \omega_1 t - \varphi_1) + \sum_\mu F_\mu \cos(\mu\theta - \mu\omega_r t - \varphi_2). \quad (13)$$

When magnetic saturation is ignored, the magnetic density can be obtained.

$$b(\theta t) = f(\theta t)\lambda(\theta t), \quad (14)$$

where $f(\theta t)$ is the air gap magnetomotive force and $\lambda(\theta t)$ is the air gap permeability.

According to Formulas (12), (13) and (14), the air-gap magnetic density expression of the motor under rated load can be obtained:

$$\begin{aligned}
 b_s(\theta, t) &= f(\theta, t)\lambda(\theta, t) \\
 &= \sum_v F_v \Lambda_0 \cos(v\theta - \omega_1 t - \varphi_1) + \sum_\mu F_\mu \Lambda_0 \cos(\mu\theta - \mu\omega_r t - \varphi_2) \\
 &\quad + \sum_v \sum_{k_1} \frac{F_v \Lambda_{k_1}}{2} \cos[(v \pm k_1 Z_1)\theta - \omega_1 t - \varphi_1] \\
 &\quad + \sum_\mu \sum_{k_1} \frac{F_\mu \Lambda_{k_1}}{2} \cos[(\mu \pm k_1 Z_1)\theta - \mu\omega_r t - \varphi_2] \\
 &\quad + \sum_v \sum_{k_2} \frac{F_v \Lambda_{k_2}}{2} \cos[(v \pm k_2 Z_2)\theta - (\omega_1 \pm k_2 Z_2 \omega_r) t - \varphi_1] \\
 &\quad + \sum_\mu \sum_{k_2} \frac{F_\mu \Lambda_{k_2}}{2} \cos[(\mu \pm k_2 Z_2)\theta - (\mu \pm k_2 Z_2) \omega_r t - \varphi_2].
 \end{aligned} \quad (15)$$

By combining Formula (15) and the Maxwell tensor method, the REF per unit area of the stator tooth surface can be obtained. The tangential component of the stator tooth flux density is ignored. The radial electromagnetic force can be obtained [17]:

$$f_r(\theta t) \approx \frac{b_s^2}{2\mu_0}, \quad (16)$$

where μ_0 is the vacuum permeability and b_s is the air-gap magnetic density.

The spatio-temporal distribution characteristics of the REF under rated load condition are shown in Table 3. According to the values of μ and v , the REF is further summarized, and the main REF components under rated load are obtained:

1. The REF component produced by the rotor MMF harmonic and the air-gap permeability constant component is $(2pn, 2nf)$.
2. The REF component produced by the interaction of rotor MMF harmonics and air gap permeability harmonics is $(2pn \pm k_2 Z_2, |2n \pm k_2 Z_2/p|f)$, where $n = 0, 1, 2, \dots, k = 1, 2, 3, \dots$
3. The REF component produced by the interaction between the stator and rotor MMF harmonics and the constant component of the air-gap permeability is $(2pn, 2nf)$.
4. The REF components produced by the interaction between the stator MMF harmonics and the constant component of the air-gap permeability are $(2pn, 2f)$ and $(2pn, 0f)$.
5. The REF components produced by the interaction of stator MMF and air gap permeability harmonics are $(2pn \pm k_1 Z_1, 2f)$ and $(2pn \pm k_1 Z_1, 0f)$.
6. The REF components produced by the interaction between stator MMF harmonics and stator slotted permeability harmonics are $(2pn \pm k_1 Z_1, 2f)$ and $(2pn \pm k_1 Z_1, 0f)$.
7. The REF component produced by the interaction between stator MMF harmonics and rotor slotted permeability harmonics is $(2pn \pm k_2 Z_2, |1 \pm 1 \mp k_2 Z_2/p|f)$.
8. The REF component produced by the interaction of the stator MMF with stator and rotor slotted permeability harmonics is $(2pn \pm k_1 Z_1 \mp k_2 Z_2, |1 \pm 1 \mp k_2 Z_2/p|f)$.
9. The REF component produced by the interaction of rotor MMF harmonics, stator MMF harmonics and stator slotted permeability harmonics is $(2pn \pm k_1 Z_1, 2nf)$.
10. The REF components produced by the interaction of rotor MMF harmonics, stator MMF harmonics and rotor slotted permeability harmonics are $(2pn \pm k_2 Z_2, |2n \pm k_2 Z_2/p|f)$ and $(2pn \pm k_2 Z_2, |1 \pm 1 \mp k_2 Z_2/p|f)$.
11. The REF components produced by the interaction of rotor MMF harmonics and stator MMF harmonics with stator and rotor slotted permeability harmonics are $(2pn \pm k_2 Z_2 \mp k_1 Z_1, |2n \pm k_2 Z_2/p|f)$ and $(2pn \pm k_1 Z_1 \mp k_2 Z_2, 2nf)$, where $n = 0, 1, 2, \dots; k_1, k_2 = 0, 1, 2, \dots$. Since $Z_1 = 72$ and $Z_2 = 56$, the spatial order and time frequency of the REF under rated load are still even.

To further verify the correctness of the above analysis, the FEM was taken to obtain the spatio-temporal distribution of the REF. In this figure, (a, bf) express the component of the radial electromagnetic force density, where the spatial component is a , the temporal component is b , and f is the fundamental wave frequency of the stator current.

According to the FFT-2D decomposition results in Fig. 5, the REF components on the rated load mainly consist of the following parts:

Part I: Generated by the interaction of the MMF harmonics with the constant component of magnetic permeability, as shown in Fig. 5, $(0,0f)$, $(8,2f)$, $(16,4f)$, $(24,6f)$, $(32,8f)$, $(40,10f)$,

Table 3. Source, spatial order and frequency characteristics of REF density under rated load

	Spatial order	Frequency characteristic
Magnetic field of rotor permanent magnet	$\mu_1 \pm \mu_2$	$(\mu_1 \pm \mu_2)f$
	$\mu_1 \pm \mu_2 \mp k_1 Z_1$	$(\mu_1 \pm \mu_2)f$
	$\mu_1 \pm \mu_2 \mp k_2 Z_2$	$(\mu_1 \pm \mu_2 \mp k_2 Z_2)f/p$
	$\mu_1 \pm \mu_2 \pm k_{11} Z_1 \mp k_{12} Z_1$	$(\mu_1 \pm \mu_2)f$
	$(\mu_1 \pm k_1 Z_1) \pm (\mu_1 \pm k_2 Z_2)$	$(\mu_1 \pm \mu_2 \mp k_2 Z_2)f/p$
	$\mu_1 \pm \mu_2 \pm k_{21} Z_2 \mp k_{22} Z_2$	$(\mu_1 \pm \mu_2 \pm k_{21} Z_2 \mp k_{22} Z_2)f/p$
The stator field interacts with the rotor permanent magnet	$\mu \pm v \pm k_2 Z_2$	$[(\mu \pm k_2 Z_2)/p \pm 1]f$
	$\mu \pm v \pm k_2 Z_2 \mp k_1 Z_1$	$[(\mu \pm k_2 Z_2)/p \pm 1]f$
	$\mu \pm v \pm k_{21} Z_2 \mp k_{22} Z_2$	$[(\mu \pm k_{21} Z_2 \mp k_{22} Z_2)/p \pm 1]f$
Stator armature field	$v_1 \pm v_2$	$f \pm f$
	$v_1 \pm v_2 \mp k_1 Z_1$	$f \pm f$
	$v_1 \pm v_2 \mp k_2 Z_2$	$(1 \pm 1 \mp k_2 Z_2/p)f$
	$v_1 \pm v_2 \pm k_{11} Z_1 \mp k_{12} Z_1$	$f \pm f$
	$v_1 \pm v_2 \pm k_1 Z_1 \mp k_2 Z_2$	$(1 \pm 1 \mp k_2 Z_2/p)f$
	$v_1 \pm v_2 \pm k_{21} Z_2 \mp k_{22} Z_2$	$[1 \pm 1 \pm (k_{21} Z_2 \mp k_{22} Z_2)/p]f$

(48,12*f*), (56,14*f*), (64,16*f*), (72,18*f*). These harmonic components are summarized and correspond to the components (2*pn*, 2*nf*) in the above analytical calculation.

Part II: Generated by the stator slot, as shown in Fig. 5, (-8,16*f*), (-16,14*f*), (-24,12*f*), (-32, 10*f*), (-40,8*f*), (-48,6*f*), (-56,4*f*), (-64,2*f*), (-72,0*f*). These harmonic components are summarized and correspond to the component (2*np* ± *kZ*₁, 2*nf*) in the above analytical calculation.

Part III: Generated by the rotor slot, as shown in Fig. 5, (-72,18*f*) and (-64,16*f*). These harmonic components are summarized and correspond to the component (2*np* ± *kZ*₂, |(2*npkZ*₂)|*f*/*p*) in the above analytical calculation.

Part IV: Generated by the interaction of the MMF harmonics and permeability harmonics on the fixed rotor side, as shown in Fig. 5, (32,26*f*), (40,28*f*), and (48,30*f*). These harmonic components are summarized and correspond to the component (2*pn* ± *kZ*₂, |2*n* ± *kZ*₂/*p*|*f*) in the above analytical calculation.

Part V: Generated by the interaction between stator MMF harmonics and stator slotted permeability harmonics, as shown in Fig. 5, (-48,0*f*), (-24,0*f*), (24,0*f*), and (48,0*f*). These harmonic components are summarized and correspond to the components (2*pn* ± *k*₁*Z*₁, 2*nf*) in the above analytical calculation.

According to the finite element analysis results, the correctness of the analytical calculation of the REF is verified.

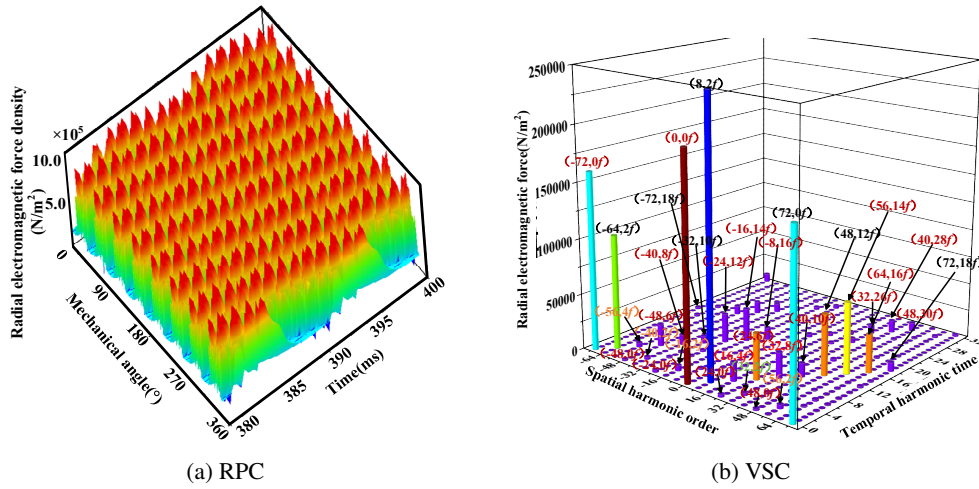


Fig. 5. Spatio-temporal distribution of the REF density and FFT-2D decomposition

While the three-phase voltage unbalance occurs, it will inevitably cause the current unbalance. The stator current contains not only the positive sequence component but also some of the negative sequence component, and the MMF is closely related to the stator current. Thus, the synthesized magnetomotive force of the stator winding under voltage unbalance can be divided into the MMF generated by the positive sequence current and negative sequence current.

$$f_m(\theta, t) = \sum_{v_{m+}} \frac{F_{m+}}{2} \cos(v_{m+}\theta - \omega_1 t - \varphi_1) + \sum_{v_{m-}} \frac{F_{m-}}{2} \cos(v_{m+}\theta + \omega_1 t - \varphi_1), \quad (17)$$

where $F_{m+}/2$ is the amplitude of the positive sequence MMF, $F_{m-}/2$ is the amplitude of the negative sequence MMF.

The air-gap MMF under the three-phase voltage unbalance of the motor can be obtained.

$$f_d = \sum_{\mu} F_{\mu} \cos(\mu\theta - \mu\omega_r t - \varphi_2) + \sum_{v_{m+}} \frac{F_{m+}}{2} \cos(v_{m+}\theta - \omega_1 t - \varphi_1) + \sum_{v_{m-}} \frac{F_{m-}}{2} \cos(v_{m+}\theta + \omega_1 t - \varphi_1). \quad (18)$$

According to Formulas (12) and (18), the expression of air-gap magnetic density under three-phase voltage unbalance can be obtained:

$$b(\theta, t) = f(\theta, t) \lambda(\theta, t) = \left\{ \begin{array}{l} \sum_{\mu} F_{\mu} \cos(\mu\theta - \mu\omega_r t - \varphi_2) + \\ \sum_{v_{m+}} \frac{F_{m+}}{2} \cos(v_{m+}\theta - \omega_1 t - \varphi_1) + \\ \sum_{v_{m-}} \frac{F_{m-}}{2} \cos(v_{m+}\theta + \omega_1 t - \varphi_1) \end{array} \right\} \left\{ \begin{array}{l} \Lambda_0 + \sum_{k_1} \Lambda_{k_1} \cos k_1 Z_1 \theta + \\ \sum_{k_2} \Lambda_{k_2} \cos k_2 Z_2 [\theta - \omega_r t] \end{array} \right\}. \quad (19)$$

The magnetic density b_{PM} produced by the rotor PM is expressed as follows:

$$\begin{aligned}
 b_{PM} = & \sum_{\mu} F_{\mu} \Lambda_0 \cos(\mu\theta - \mu\omega_r t - \varphi_2) \\
 & + \sum_{\mu} \sum_{k_1} \frac{F_{\mu} \Lambda_{k_1}}{2} \cos[(\mu \pm k_1 Z_1)\theta - \mu\omega_r t - \varphi_2] \\
 & + \sum_{\mu} \sum_{k_2} \frac{F_{\mu} \Lambda_{k_2}}{2} \cos[(\mu \pm k_2 Z_2)\theta - (\mu \pm k_2 Z_2)\omega_r t - \varphi_2].
 \end{aligned} \quad (20)$$

The magnetic density b_m generated by the stator armature current is expressed as follows:

$$\begin{aligned}
 b_m = & \sum_{v_{m+}} \frac{F_{v_{m+}} \Lambda_0}{2} \cos(v_{m+}\theta - \omega_1 t - \varphi_1) \\
 & + \sum_{v_{m-}} \frac{F_{v_{m-}} \Lambda_0}{2} \cos(v_{m+}\theta + \omega_1 t - \varphi_1) \\
 & + \sum_{v_{m+}} \sum_{k_1} \frac{F_{v_{m+}} \Lambda_{k_1}}{4} \cos[(v_{m+} \pm k_1 Z_1)\theta - \omega_1 t - \varphi_1] \\
 & + \sum_{v_{m-}} \sum_{k_1} \frac{F_{v_{m-}} \Lambda_{k_1}}{4} \cos[(v_{m+} \pm k_1 Z_1)\theta + \omega_1 t - \varphi_1] \\
 & + \sum_{v_{m+}} \sum_{k_2} \frac{F_{v_{m+}} \Lambda_{k_2}}{4} \cos[(v_{m+} \pm k_2 Z_2)\theta - (\omega_1 \pm k_2 Z_2 \omega_r) t - \varphi_1] \\
 & + \sum_{v_{m-}} \sum_{k_2} \frac{F_{v_{m-}} \Lambda_{k_2}}{4} \cos[(v_{m-} \pm k_2 Z_2)\theta + (\omega_1 \mp k_2 Z_2 \omega_r) t - \varphi_1].
 \end{aligned} \quad (21)$$

By combining Formulas (20), (21) and the Maxwell tensor method, the tangential component of the stator tooth surface flux density can be ignored. The REF under three-phase voltage unbalance can be obtained:

$$f_r(\theta t) = \frac{(b_{PM} + b_m)^2}{2\mu_0} = \frac{b_{PM}^2}{2\mu_0} + \frac{b_{PM} b_m}{\mu_0} + \frac{b_m^2}{2\mu_0}, \quad (22)$$

where b_{PM} is the flux density produced by the rotor, b_m is the flux density produced by the stator windings.

The source, spatial order and frequency characteristics of the REF under voltage unbalance are shown in Table 4. The REF amplitude produced by the harmonic interaction of magnetic permeability can be ignored.

It can be seen from Fig. 6 that when voltage unbalance occurs, compared with the spatio-temporal harmonic distribution of the REF under rated load, the newly added spatio-temporal harmonic components are as follows: $(8, 0f)$, $(-8, 0f)$, $(-64, 0f)$, $(64, 0f)$, $(-72, 2f)$, $(72, 2f)$, $(56, 12f)$, $(48, 14f)$, $(64, 14f)$ and $(56, 16f)$, where $(8, 0f)$ and $(64, 0f)$ correspond to the analytic analysis expression: $(v_{m+} \pm v_{m-} f)$; $(-8, 0f)$ and $(-64, 0f)$ correspond to the analytic analysis expression: $(v_{m+} \pm v_{m-} \pm k_1 Z_1 f)$; $(-72, 2f)$ and $(72, 2f)$ correspond to the analytic analysis expression: $(v_{m+} \pm v_{m-} \pm k_1 Z_1, 2f)$; $(48, 14f)$ and $(64, 14f)$ correspond to the analytic analysis expression: $[v_{m+} \pm v_{m-} \pm k_2 Z_2, (k_2 Z_2 / p) f]$; $(56, 12f)$ and $(56, 16f)$ correspond to the analytic analysis expression: $(v_{m+} \pm v_{m-} \pm k_2 Z_2 |k_2 Z_2 / p \pm 2| f)$, and the correctness of the above theoretical analysis is validated.

Table 4. Source, spatial order and frequency characteristics of electromagnetic force density under three-phase voltage imbalance

	Spatial order	Frequency characteristic
Stator armature field	$v_{m1+} \pm v_{m2+}$	0, 2
	$v_{m1-} \pm v_{m2-}$	0, 2
	$v_{m+} \pm v_{m-}$	0, 2
	$v_{m1+} \pm v_{m2+} \pm k_1 Z_1$	0, 2
	$v_{m+} \pm v_{m-} \pm k_1 Z_1$	0, 2
	$v_{m1+} \pm v_{m2+} \pm k_2 Z_2$	$0, 2 \pm k_2 Z_2/p$
	$v_{m+} \pm v_{m-} \pm k_2 Z_2$	$0, 2 \pm k_2 Z_2/p$
The stator magnetic field interacts with the permanent magnet field	$v_{m+} \pm \mu$	$1 \pm \mu$
	$v_{m-} \pm \mu$	$1 \pm \mu$
	$v_{m+} \pm \mu \pm k_1 Z_1$	$1 \pm \mu$
	$v_{m-} \pm \mu \pm k_1 Z_1$	$1 \pm \mu$
	$v_{m+} \pm \mu \pm k_2 Z_2$	$1 \pm \mu \pm k_2 Z_2/p$
	$v_{m-} \pm \mu \pm k_2 Z_2$	$1 \pm \mu \pm k_2 Z_2/p$
Magnetic field of rotor permanent magnet	$\mu_1 \pm \mu_2$	$(\mu_1 \pm \mu_2)$
	$\mu_1 \pm \mu_2 \mp k_1 Z_1$	$(\mu_1 \pm \mu_2)$
	$\mu_1 \pm \mu_2 \mp k_2 Z_2$	$(\mu_1 \pm \mu_2 \mp k_2 Z_2)/p$
	$\mu_1 \pm \mu_2 \pm k_{11} Z_1 \mp k_{12} Z_1$	$(\mu_1 \pm \mu_2)$
	$(\mu_1 \pm k_1 Z_1) \pm (\mu_1 \pm k_2 Z_2)$	$(\mu_1 \pm \mu_2 \mp k_2 Z_2)/p$
	$\mu_1 \pm \mu_2 \pm k_{21} Z_2 \mp k_{22} Z_2$	$(\mu_1 \pm \mu_2 \pm k_{21} Z_2 \mp k_{22} Z_2)/p$

According to the theory of electromagnetic vibration, the vibration acceleration of the motor is proportional to the amplitude of the REF and inversely proportional to the fourth square of the spatial order. Thus, the impact of low-order REF with large amplitude on electromagnetic vibration should be emphasized, and the REF amplitude under different voltage unbalance degrees should be analyzed by the FEM, are shown in Fig. 7.

According to Fig. 7, the REF amplitudes of 0-order and 8-order of the motor are large. Based on the above analysis, the vibration magnitude of the machine is inversely proportional to the fourth square of the spatial order of the electromagnetic force wave, so the spatial order of the non-zero electromagnetic force wave that plays a major role in vibration is 8. When the voltage unbalance occurs, the amplitude of 0-order and 8-order REF obviously changes, and its amplitude increases with the increase in the VUD. Therefore, the voltage unbalance further affects the electromagnetic vibration by affecting the amplitude of the low-order REF of the motor.

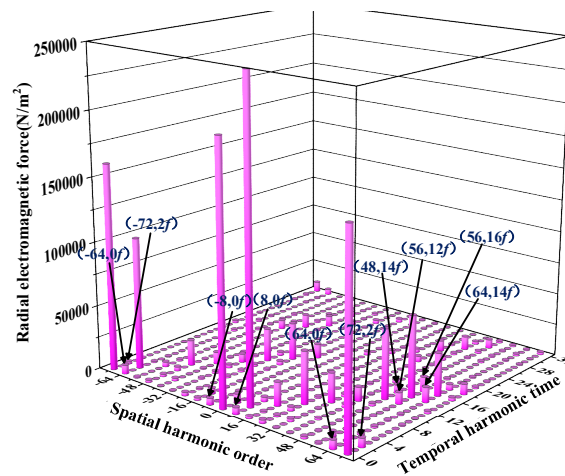


Fig. 6. Temporal and spatial harmonic distribution of the REF under three-phase voltage unbalance

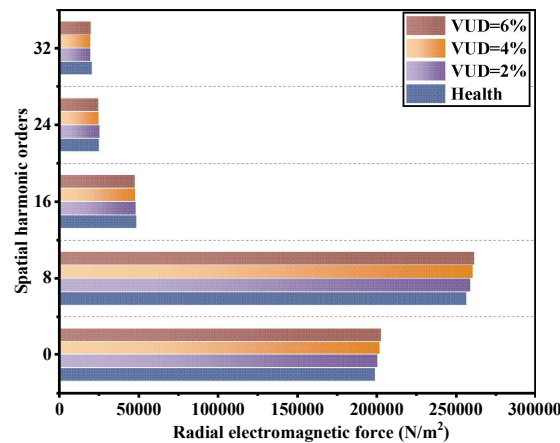


Fig. 7. Spatial harmonic order of the REF under different VUDs

5. Modal analysis

Modal is an intrinsic vibration property of mechanical structure, and each modal has a specific modal frequency and modal shape. However, when the modal frequency is close to the frequency of the electromagnetic force wave, the motor will resonate which causes the vibration to intensify. The modal frequency is related to the quality and stiffness of the motor structure, and reasonable parameters should be selected in the motor design to keep the modal frequency away from the electromagnetic wave frequency to prevent the occurrence of resonance. Modal analysis methods mainly include the finite element method and analytical method. The FEM has more advantages than the analytical method in calculation accuracy. Therefore, the FEM is taken to analyze the modal in this paper, and the first seven modal shapes and frequencies of the stator core of the motor are obtained, as shown in Fig. 8.

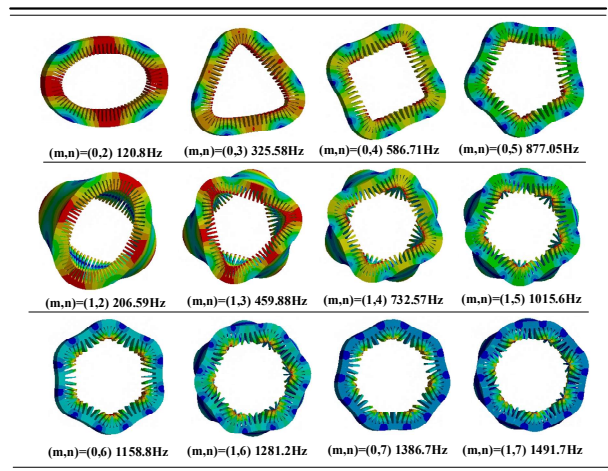


Fig. 8. Stator modal shapes and frequencies

According to Fig. 8, the natural frequency of the stator core increases with the increase in the modal order. Due to the large axial length of the motor, the inner diameter of the rotor and stator and the axial length of the iron core, and the large mass, the natural frequency of the motor is small. Therefore, the natural frequency and low-frequency electromagnetic force should be considered in the design of the motor to avoid resonance.

6. Harmonic response analysis

Through the above analysis of the REF, the low-order spatial harmonics of the REF is greatly affected by the voltage unbalance, and further affect the electromagnetic vibration of the motor. To reveal the influence mechanism of voltage unbalance on the electromagnetic vibration, the VUDs is 2%, 4% and 6% for research. The vibration amplitude of the motor under different VUDs is compared, and the results are shown in Fig. 9.

According to Fig. 9, the vibration amplitude of the motor is large at 800 Hz, 900 Hz and 1000 Hz. At $16f$ (800 Hz), the spatial order corresponding to $16f$ is 64. Based on the stator tooth modulation theory, while the force wave order is greater than $Z_1/2$, the high-order electromagnetic force wave will be modulated to the low-order REF, and the order of the modulated REF is $\lambda - nZ_1$. Thus, the 64-order electromagnetic force of the 72-slot 8-pole motor studied in this study is modulated by 72 teeth to the 8-order REF, which is the minimum non-zero spatial order radial electromagnetic wave in the 8-pole motor of the prototype in this paper.

At $18f$ (900 Hz), it is because the spatial order corresponding to $18f$ is 72. The 72-order REF of the 72-slot 8-pole motor studied in this paper is modulated by 72 teeth to the 0-order REF, which causes the zero-order vibration of the stator yoke.

At $20f$ (1000 Hz), although the REF amplitude corresponding to this frequency is small, it is close to the fifth-order modal frequency (1015.6 Hz), which produces resonance and intensification of vibration.

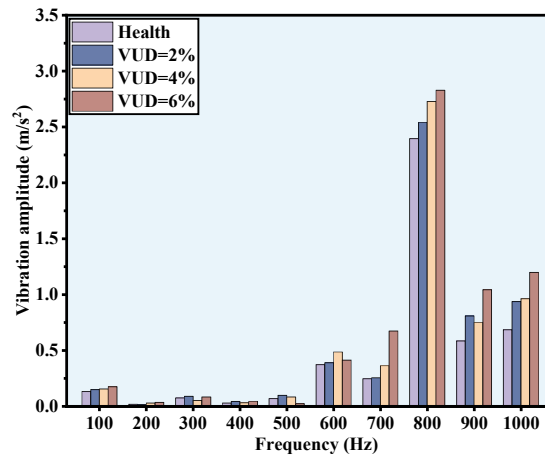


Fig. 9. Vibration amplitude of the motor under different VUDs

When the voltage unbalance occurs, its vibration amplitude changes significantly at 600 Hz, 700 Hz, 800 Hz, 900 Hz, 1000 Hz, and at 100 Hz, 700 Hz, 800 Hz, 1000 Hz, the motor vibration amplitude increases with the increase in the VUD. Therefore, it is concluded that the three-phase voltage unbalance has a greater effect on the electromagnetic vibration of the motor. When the VUD is 6%, a vibration acceleration amplitude of 800 Hz and 900 Hz increases by 18.03% and 78.57%, respectively.

7. Conclusion

The impact of three-phase voltage unbalance on electromagnetic and vibration performance of the HVLS PMSM is studied in this paper, including torque ripple, torque harmonic frequency, REF, modal and vibration harmonic response. The following conclusions can be drawn:

Torque ripple increases with the increase in the VUD, when the motor is operating normally, there are only $6k$ harmonic torque components, when the voltage unbalance occurs, there are $2k$ harmonic torque components in the torque.

The REF spatial harmonic order under rated load is $2pn$, and the temporal harmonic time is $2nf$. When the voltage unbalance occurs, the newly added spatio-temporal harmonic components are: $(8, 0f)$, $(-8, 0f)$, $(-64, 0f)$, $(64, 0f)$, $(-72, 2f)$, $(72, 2f)$, $(56, 12f)$, $(48, 14f)$, $(64, 14f)$, $(56, 16f)$, and the correctness of the above theoretical analysis is validated. In addition, the spatial harmonic amplitude of the radial electromagnetic force in the case of voltage unbalance increases significantly, especially the spatial 8-order REF which has a greater effect on electromagnetic vibration.

Combined with the analysis of the modal and the REF, the vibration amplitude of the motor at 800 Hz, 900 Hz and 1000 Hz is large, which verifies the analysis results of the REF and modal. At 100 Hz, 700 Hz, 800 Hz and 1000 Hz, the vibration amplitude increases with the increase in the VUD.

At last, it is concluded that the electromagnetic performance and vibration of the motor are greatly affected by the three-phase voltage unbalance. When the VUD is 6%, the vibration acceleration amplitude of 800 Hz and 900 Hz increases by 18.03% and 78.57%, respectively.

Acknowledgements

This work was supported in part by the National Natural Science Foundation of China under Grant 52177063, and in part by Excellent Young Scholars Project of Henan Province under Grant 232300421070, and in part by the University Science and Technology Innovation Talent Support Program of Henan province under Grant 23HASTIT026, and in part by the Science and Technology Project of Henan Province under Grant 232102220080, 222102320074, 242102221002.

References

- [1] Lyskawinski W., *Comparative analysis of energy performance of squirrel cage induction motor, line-start synchronous reluctance and permanent magnet motors employing the same stator design*, Archives of Electrical Engineering, vol. 69, no. 4, pp. 967–981 (2020), DOI: [10.24425/ae.2020.134642](https://doi.org/10.24425/ae.2020.134642).
- [2] Zawilak T., *Influence of rotor's cage resistance on demagnetization process in the line start permanent magnet synchronous motor*, Archives of Electrical Engineering, vol. 69, no. 2, pp. 249–258 (2020), DOI: [10.24425/ae.2020.133023](https://doi.org/10.24425/ae.2020.133023).
- [3] Shen J.X., Li P., Jin M.J. et al., *Investigation and countermeasures for demagnetization in line start permanent magnet synchronous motors*, IEEE Transactions on Magnetics, vol. 49, no. 7, pp. 4068–4071 (2013), DOI: [10.1109/TMAG.2013.2244582](https://doi.org/10.1109/TMAG.2013.2244582).
- [4] Kang G.H., Hur J., Nam H. et al., *Analysis of irreversible magnet demagnetization in line-start motors based on the finite-element method*, IEEE Transactions on Magnetics, vol. 39, no. 3, pp. 1488–1491 (2003), DOI: [10.1109/TMAG.2003.810330](https://doi.org/10.1109/TMAG.2003.810330).
- [5] Wang Dao-han, Wang Xiu-he, Zhong Hui, Shen H., *Simulation of three-phase line-start permanent magnet synchronous motor fed by unbalanced voltages*, Proceedings of the CSEE, vol. 25, no. 19, pp. 152–156 (2005), DOI: [10.13334/j.0258-8013.pcsee.2005.19.029](https://doi.org/10.13334/j.0258-8013.pcsee.2005.19.029).
- [6] Tang Xu, Wang Xiuhe, Li Ying, *Demagnetization Study for Line-start Permanent Magnet Synchronous Motor Fed By Three-phase Unbalanced Voltages*, Proceedings of the CSEE, vol. 35, no. 23, pp. 6172–6178 (2015), DOI: [10.13334/j.0258-8013.pcsee.2015.23.025](https://doi.org/10.13334/j.0258-8013.pcsee.2015.23.025).
- [7] Ugale R.T., BalaKrishna Y., Chaudhari B.N., *Effects of short power interruptions and voltage sags on the performance of line start permanent magnet synchronous motor*, 2008 4th IET Conference on Power Electronics, Machines and Drives, York, pp. 184–188 (2008), DOI: [10.1049/cp:20080508](https://doi.org/10.1049/cp:20080508).
- [8] Hosseinzadeh Soreshjani M., Haghparast M., *Classical Direct Torque Control performance of Line Start PM Synchronous Motor for different conditions*, International Transactions on Electrical Energy Systems, vol. 25, no. 11, pp. 2595–2620 (2015), DOI: [10.1002/etep.1973](https://doi.org/10.1002/etep.1973).
- [9] Ching-Yin Lee, Bin-Kwie Chen, Wei-Jen Lee, Yen-Feng Hsu, *Effects of various unbalanced voltages on the operation performance of an induction motor under the same voltage unbalance factor condition*, IEEE Industrial and Commercial Power Systems Technical Conference, Philadelphia, USA, pp. 51–59 (1997), DOI: [10.1109/ICPS.1997.595989](https://doi.org/10.1109/ICPS.1997.595989).
- [10] Wang Xiu-he, Yang Yu-bo, Fu Da-jin J., *Analysis of Three-phase Induction Motor Fed by Unbalanced Voltages with Transient Model*, Proceedings of the CSEE, vol. 23, no. 2, pp. 130–135 (2003), DOI: [10.13334/j.0258-8013.pcsee.2003.02.027](https://doi.org/10.13334/j.0258-8013.pcsee.2003.02.027).
- [11] Yaw-Juen Wang, *An analytical study on steady-state performance of an induction motor connected to unbalanced three-phase voltage*, 2000 IEEE Power Engineering Society Winter Meeting, Singapore, pp. 159–164 (2000), DOI: [10.1109/PESW.2000.849947](https://doi.org/10.1109/PESW.2000.849947).
- [12] Kersting W.H., *Causes and effects of unbalanced voltages serving an induction motor*, IEEE Transactions on Industry Applications, vol. 37, no. 1, pp. 165–170 (2001), DOI: [10.1109/28.903142](https://doi.org/10.1109/28.903142).

- [13] Gonzalez-Cordoba J.L., Osornio-Rios R.A., Granados-Lieberman D. et al., *Correlation Model Between Voltage Unbalance and Mechanical Overload Based on Thermal Effect at the Induction Motor Stator*, IEEE Transactions on Energy Conversion, vol. 32, no. 4, pp. 1602–1610 (2017), DOI: [10.1109/TEC.2017.2706194](https://doi.org/10.1109/TEC.2017.2706194).
- [14] Chai Feng, Geng Lina, Pei Yulong, *Axial Split Phase Integral Slot Concentrated Winding Permanent Magnet Fault Tolerant Motors and Its Investigation of Interturn Short Circuit Faults Suppression*, Proceedings of the CSEE, vol. 43, no. 13, pp. 5203–5218 (2023), DOI: [10.13334/j.0258-8013.pcsee.220432](https://doi.org/10.13334/j.0258-8013.pcsee.220432).
- [15] Yang G.L., Chen S., Qiao J.W. et al., *The influence of ITSF on vibration of high voltage Line-Start permanent magnet synchronous motor*, COMPEL, vol. 43, no. 2, pp. 301–317 (2024), DOI: [10.1108/COMPEL-11-2023-0610](https://doi.org/10.1108/COMPEL-11-2023-0610).
- [16] Yang C.X., Wang Y.M., Qiu H.B. et al., *Electromagnetic Vibration of High-Voltage Line-Start Permanent Magnet Synchronous Motor with Demagnetization Fault*, Journal of Electrical Engineering and Technology, vol. 19, no. 7, pp. 4143–4158 (2024), DOI: [10.1007/s42835-024-01828-5](https://doi.org/10.1007/s42835-024-01828-5).
- [17] Fu W.N., Ho S.L., *A Quantitative Comparative Analysis of a Novel Flux-modulated Permanent-magnet Motor for Low-speed Drive*, IEEE Trans. Magn., vol. 46, no. 1, pp. 127–134 (2010), DOI: [10.1109/TMAG.2009.2030677](https://doi.org/10.1109/TMAG.2009.2030677).